

Sextets in four-terminal Josephson junctions

Miriam Rike Ebert,¹ David Christian Ohnmacht,^{1,*} Wolfgang Belzig,¹ and Juan Carlos Cuevas^{2,3}

¹*Fachbereich Physik, Universität Konstanz, D-78457 Konstanz, Germany*

²*Departamento de Física Teórica de la Materia Condensada,
Universidad Autónoma de Madrid, 28049 Madrid, Spain*

³*Condensed Matter Physics Center (IFIMAC), Universidad Autónoma de Madrid, 28049 Madrid, Spain*

(Dated: August 1, 2025)

Multiterminal superconducting junctions have revitalized the investigation of the Josephson effect. One of the most interesting aspects of these hybrid systems is the occurrence of multi-Cooper pair tunneling processes that have no analog in two-terminal devices. Such correlated tunneling events are also intimately connected to the Andreev bound states (ABSs) supported by these structures. Josephson junctions with four superconducting terminals have attracted special attention because they are predicted to support ABSs with nontrivial topological properties. Here, we present a theoretical study of *sextets*, which are correlated tunneling processes involving three Cooper pairs and four different superconducting terminals. We investigate how sextets can be identified from the analysis of the current-phase relation, we show how sextets are connected to the hybridization of ABSs, and we discuss their existence in recent experiments on four-terminal devices realized in hybrid Al/InAs heterostructures.

I. INTRODUCTION

The dc Josephson effect, i.e., the ability of a superconducting junction to sustain a nondissipative current, is one of the most emblematic phenomena in the field of superconductivity [1, 2]. The modern view of the dc Josephson effect is that a superconducting phase difference across a Josephson junction generates Andreev bound states (ABSs), which in turn mediate the Cooper pair transfer responsible of the supercurrent flow [3, 4]. The exact current-phase relation (CPR) of a superconducting hybrid device depends on many details (materials, junction dimensions, etc.), and its connection with the ABS energy spectra has been widely investigated in two-terminal Josephson junctions (JJs), see Refs. [5–19] for recent examples.

The advent of multiterminal Josephson junctions (MTJJs) has provided a new impetus to the study of the Josephson effect and related issues [20–25]. The interest in these hybrid systems is manifold. Thus, for instance, these MTJJs sustain ABSs that depend on a number of superconducting phase differences, thus forming energy bands that may exhibit unique properties and eventually serve as a new type of qubits. In particular, it has been theoretically predicted that MTJJs are ideal platforms for band-structure engineering to realize topological systems [26–39]. In fact, the first experimental steps in this direction have already been reported making use of tunneling spectroscopy [40, 41]. Another topic of interest in the context of MTJJs is the use of these hybrid structures to investigate so-called Josephson diodes [42]. Additionally, it has also been recently predicted that the ABSs in MTJJs could enable the study of engineered non-Hermitian topologies [43].

From the standpoint of quantum transport, MTJJs are also very interesting because they enable the exploration of complex tunneling processes that have no two-terminal analogs. A good example is the concept of a *quartet*, which consists in the simultaneous tunneling of two Cooper pairs originating in a given superconducting terminal and exiting the structure via two different electrodes [44, 45]. These tunneling events give rise to a very peculiar phase dependence in the CPR that reflects the correlated, multiterminal character of these processes [46–49]. Thus far, most of the experimental efforts to observe these quartet processes have been based on probing the system response as a function of two bias currents or voltages [50–53]. A notable exception is Ref. [54] in which quartet signatures were found directly in the ABS tunneling spectra of a three-terminal device employing the so-called *quartet tomography*, which consists of a Fourier analysis of either the CPR or the ABS band structure. In that work, it was also shown that the occurrence of quartets is closely related to the hybridization of the ABSs. This fact illustrated that quartets are not only of fundamental interest, but also that their analysis serves to rigorously establish if a MTJJ exhibits genuine physics beyond that of two-terminal devices.

The goal of this work is to extend the theoretical analysis of correlated tunneling processes to the case of four-terminal devices. These MTJJs have become the holy grail of this field because, as mentioned above, it has been predicted that they can be used to realize topologically nontrivial phases in the three-dimensional ABS band structure, in particular with the appearance of Weyl nodes [27]. In this context, we focus here on the analysis of *sextets*, which are processes that involve the simultaneous tunneling of three Cooper pairs that involve up to four different superconducting terminals. To be precise, we focus here on short junctions, with dimensions smaller than the superconducting coherence length. We make use of relatively simple models to illustrate the nature

* david.ohnmacht@uni-konstanz.de

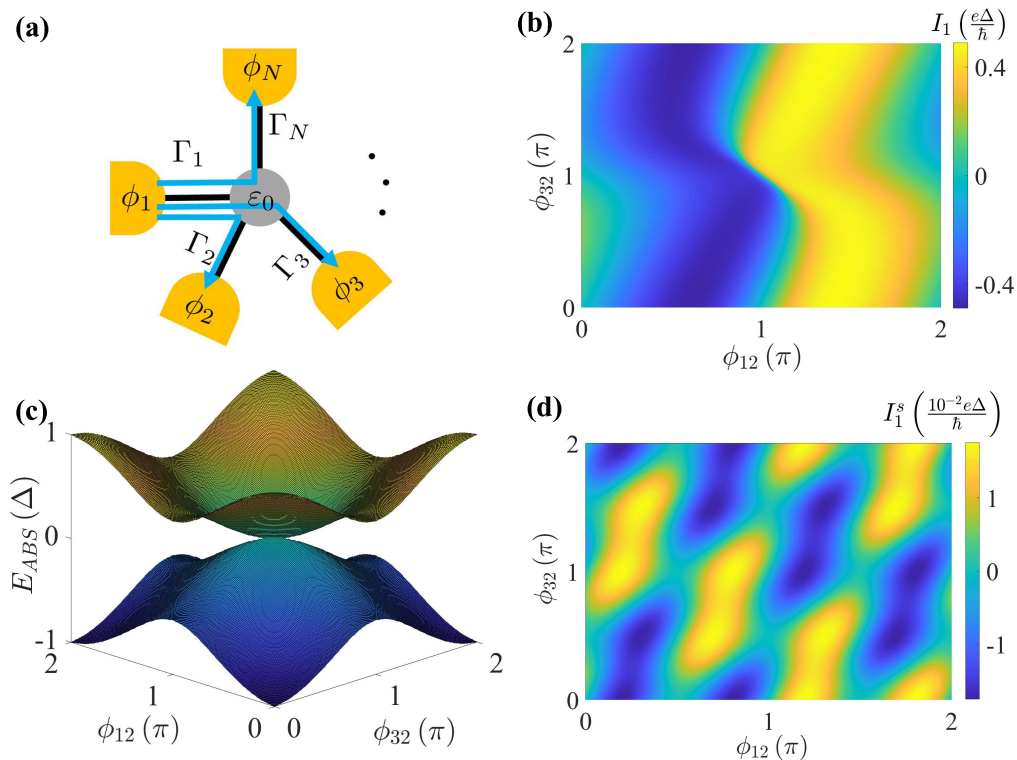


FIG. 1. (a) Schematics of the single-dot model. A single-level of energy ϵ_0 is coupled to N superconducting terminals with phases ϕ_j . The parameter Γ_j describes the strength of the coupling between the dot and lead j . The blue lines describe a sextet process in which 3 Cooper pairs tunnel simultaneously from terminal 1 and each then leaves the hybrid structure via a different electrode. (b) Example of the current-phase relation $I_1(\phi_{12}, \phi_{32}, \phi_{42})$ for the model in (a) with four identical leads with energy gap Δ . The different parameters are: $\Gamma_j = 5\Delta$ for $j \in \{1, 2, 3, 4\}$, $\epsilon_0 = 0$, $\phi_4 = 0$, and $k_B T = 0.01\Delta$. (c) The corresponding phase dependence of the ABSs for the example in (b). (d) The total contribution of the four sextets to the current I_1 in the example of panel (b).

of these tunneling events, to discuss under which conditions they can be observed in the CPR, and we show how they are related to the hybridization of the ABSs in these MTJJs. Finally, we also discuss the possible existence of sextets in very recent experiments performed in four-terminal JJs realized in hybrid Al/InAs heterostructures [41].

The rest of this manuscript is organized as follows. In Sec. II we analyze a model of a four-terminal Josephson junction in which the normal region is made of a single quantum level. This simple model allows us to illustrate the character of the sextets, as well as to discuss the conditions for their observation in the CPR. Section III is devoted to the analysis of a double-dot model with the goal to elucidate the connection between the occurrence of sextets and the hybridization of the ABSs. In Sec. IV we investigate the occurrence of sextets in a model that was recently employed to describe the ABS spectra in four-terminal JJs realized in a hybrid Al/InAs heterostructure [41]. We summarize the main conclusions of this work in Sec. V. We also include two appendices to describe the technical details concerning the calculation of the supercurrent in the different models presented in this work, see

Appendix A, and to provide additional results obtained with an insightful approximation, see Appendix B.

II. SEXTET TOMOGRAPHY: SINGLE-DOT MODEL

Let us start our discussion by defining what we mean by a sextet and how it can be identified in the CPR of a MTJJ. For this purpose, it is didactic to analyze the simple model shown in Fig. 1(a). In this model, a single-level, noninteracting quantum dot is coupled to N superconducting leads. The energy of the spin-degenerate level is denoted by ϵ_0 and the electrodes are s -wave superconductors with energy gaps Δ_j and superconducting phases ϕ_j ($j = 1, \dots, N$). The coupling between the normal region and the lead j is described by the tunneling rate Γ_j (with dimensions of energy). Our objective is to calculate the nondissipative, zero-bias current flowing through the different terminals as a function of the superconducting phases ϕ_j . To this end, we make use of Green's function techniques and our starting point are the (dimensionless) retarded

and advanced Green's functions of the leads, which in a 2×2 Nambu representation read $\hat{g}_j^{r/a}(E) = g_j^{r/a} \hat{\tau}_0 + f_j^{r/a} e^{i\phi_j} \hat{\tau}_3$, with $g_j^{r/a} = -(E \pm \eta)/\sqrt{\Delta_j^2 - (E \pm \eta)^2}$ and $f_j^{r/a} = -\Delta_j/\sqrt{\Delta_j^2 - (E \pm \eta)^2}$. Here, E is the energy, $\eta = 0^+$, and $\tau_{0,1,3}$ are Pauli matrices. As shown in Appendix A, one can write the current flowing through lead i as $I_i = \sum_{j \neq i} I_{ij}$, where I_{ij} is given by

$$I_{ij} = \frac{8e}{h} \Gamma_i \Gamma_j \sin(\phi_{ji}) \int_{-\infty}^{\infty} \Im \left\{ \frac{f_i^a(E) f_j^a(E)}{D(E, \phi)} \right\} n_F(E) dE, \quad (1)$$

where $\phi_{ji} = \phi_j - \phi_i$, $n_F(E)$ is the Fermi function, $\phi = (\phi_1, \dots, \phi_N)$, and $D(E, \phi)$ is given by

$$D(E, \phi) = \left[E - \epsilon_0 - \sum_k \Gamma_k g_k^a \right] \left[E + \epsilon_0 - \sum_k \Gamma_k g_k^a \right] - \left[\sum_k \Gamma_k f_k^a e^{i\phi_k} \right] \left[\sum_k \Gamma_k f_k^a e^{-i\phi_k} \right]. \quad (2)$$

The ABS energies as a function of the different superconducting phases are obtained from the condition $D(E, \phi) = 0$.

In this work, we are interested in four-terminal devices and for concreteness, we shall focus on the analysis of I_1 , the supercurrent flowing through terminal 1. This current depends on three phase differences, chosen ϕ_{12} , ϕ_{32} , and ϕ_{42} , and can be written as the following Fourier series

$$I_1(\phi_{12}, \phi_{32}, \phi_{42}) = \sum_{l,n,m} c_{lnm} \sin(l\phi_{12} + n\phi_{32} + m\phi_{42}). \quad (3)$$

In a four-terminal Josephson junction, a sextet is a correlated tunneling process in which 3 Cooper pairs tunnel into the normal region from a given terminal and each of them exits the structure through a different terminal. This multi-Cooper pair tunneling process gives a contribution to the current that depends on a combination of phases of the type $\phi_l^s = \phi_i + \phi_j + \phi_k - 3\phi_l$. Here, l corresponds to the terminal from which the 3 Cooper pairs originate and all indices are different. In a four-terminal device, there are four sextets, each one originating from a different terminal. The contribution of sextet l to I_1 is given by $S_l \sin(\phi_l^s)$, where $S_1 = c_{-311}$, $S_2 = c_{111}$, $S_3 = c_{1-31}$, and $S_4 = c_{11-3}$. The first contribution, S_1 , corresponds to the sextet in which three Cooper pairs enter the normal region from terminal 1 and exit separately via the other 3 terminals, see Fig. 1(a). The other three sextets have similar interpretations. As shown in Appendix A, one can do a perturbative analysis of Eq. (1) to show that the Fourier coefficients determining the sextets are given to leading order in the Γ parameters by: $c_{-311} = 3A_1$, $c_{111} = -A_2$, $c_{1-31} = -A_3$, $c_{11-3} = -A_4$,

where

$$A_l = \frac{4e}{h} \Gamma_l^3 \Gamma_i \Gamma_j \Gamma_k \int_{-\infty}^{\infty} dE n_F(E) \times \Im \left\{ \frac{[f_l^a(E)]^3 f_i^a(E) f_j^a(E) f_k^a(E)}{(E^2 - \epsilon_0^2)^3} \right\}. \quad (4)$$

This equation supports the interpretation that a sextet of the type $\phi_1^s = \phi_2 + \phi_3 + \phi_4 - 3\phi_1$ involves the injection of three Cooper pairs from terminal 1 that are transferred separately to leads 2, 3 and 4. It is important to stress that, apart from these sextet contributions, the supercurrent I_1 has also contributions from all the typical two- and three-terminal processes. In any case, Eq. (3) provides a direct way to extract the sextet contributions, which simply consists in performing a Fourier analysis of the CPR [54]. On the other hand, the form of Eq. 3 is completely general for a four-terminal device, i.e., it is independent of the structure of the normal region, which only affects the individual coefficients c_{lnm} in Eq. 3.

We illustrate the results for this single-dot model in Fig. 1(b) where we show the CPR I_1 for the parameters specified in the figure caption. On the other hand, and to illustrate the role of the sextets, we display in Fig. 1(d) the supercurrent exclusively due to the four sextets, which was simply determined by selecting the corresponding Fourier coefficients in Eq. (3). Notice that these correlated tunneling processes give a non-negligible contribution to the total current. As mentioned above, it is important to emphasize that the sextet contributions are accompanied by many others, which include single- and multi-Cooper pair tunneling between pairs of terminals and quartets involving three terminals. This is the reason why these multi-Cooper pair tunneling processes are not easy to identify solely by exploring the critical current of these junctions.

It is important to recall that in these coherent superconducting structures, the supercurrent is mainly carried by the ABSs generated by the superconducting phase difference. As stated above, the energies of those bound states can be obtained from the condition $D(E, \phi) = 0$.

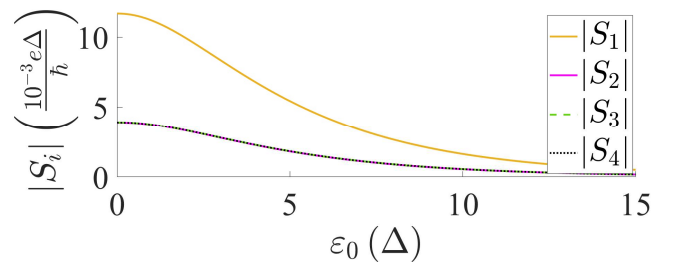


FIG. 2. Evolution of the magnitude of the sextet coefficients as a function of the level position in single-dot model of Fig. 1 with four terminals. The parameters other than the level position are the same as in Fig. 1(b). Notice that there is a three-fold degeneracy of these coefficients.

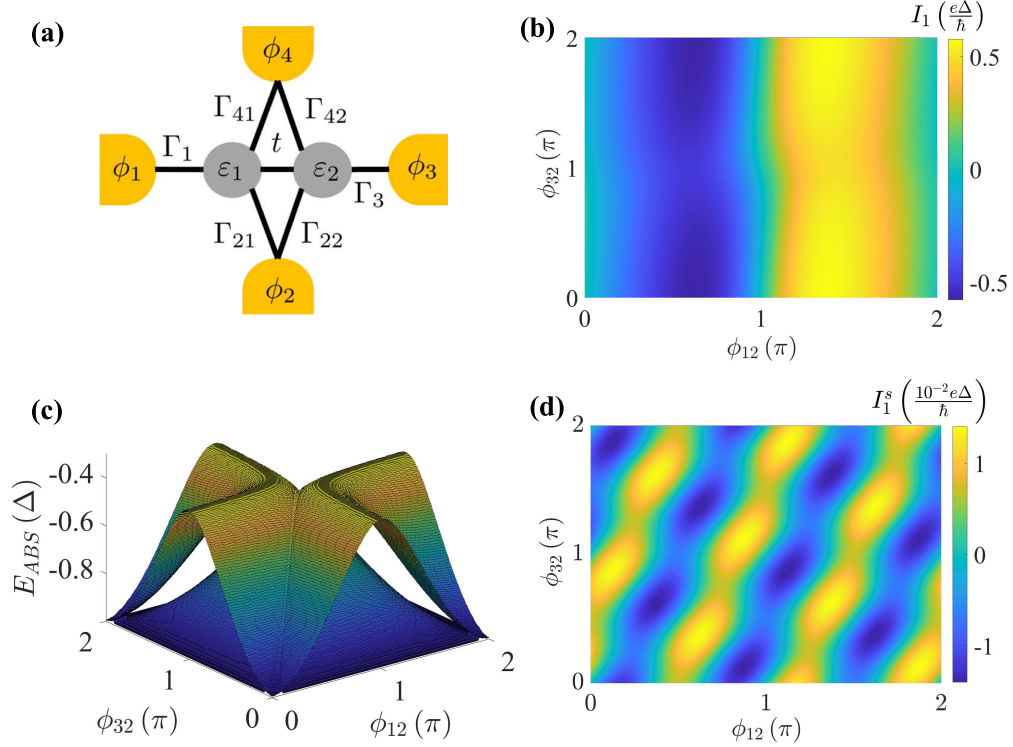


FIG. 3. (a) Schematics of the two-dot model. Two single-level quantum dots of energies ϵ_1 and ϵ_2 are coupled to four superconducting terminals with phases ϕ_j . The parameters Γ describe the strength of the coupling between the levels and the leads, as shown in this schematics. In particular, leads 2 and 4 are coupled to the two dots. The parameter t describes the interdot coupling and controls the degree of hybridization of the ABSs. (b) Example of the current-phase relation $I_1(\phi_{12}, \phi_{32}, \phi_{42})$ for the model in (a) with four identical leads with energy gap Δ . The different parameters are: $\Gamma_j = 5\Delta$ for $j \in \{1, 21, 22, 3, 41, 42\}$, $\epsilon_1 = \epsilon_2 = 0$, $t = 5\Delta$, $\phi_4 = 0$, and $k_B T = 0.01\Delta$. (c) The corresponding phase dependence of the ABSs for the example in (b). We only show here the two states below the Fermi energy (there is electron-hole symmetry). (d) The total contribution of the four sextets to the current I_1 in the example of panel (b).

In Fig. 1(c) we show the ABSs corresponding to the four-terminal example of panel (b). Notice that ABSs form a pair of energy bands with electron-hole symmetry. In these MTJJ, the zero-temperature current I_1 is obtained from the energies $E_{ABS}^{(k)}$ of the occupied ABSs as follows

$$I_1(\phi) = \frac{2e}{h} \sum_k \frac{\partial E_{ABS}^{(k)}(\phi)}{\partial \phi_1}, \quad (5)$$

where the factor 2 is due to spin degeneracy. We have verified that, in all the examples shown in this work, we can reconstruct the CPR using Eq. (5). This demonstrates that the supercurrent is carried by the ABSs with no contributions from the continuum. As discussed in Ref. [54], this connection between ABSs and supercurrent suggests another protocol to identify sextets, which consists in the Fourier analysis of the ABS spectrum. That is a viable strategy in those experiments in which the ABS spectrum is measured, e.g., via tunneling spectroscopy [40]. This was explicitly demonstrated in Ref. [54]. In this work, we shall not pursue this strategy and focus on the sextet signatures directly in the CPR.

Once we have established that sextets may exist in co-

herently coupled multi-terminal systems, the next natural issue is to find out in which range of parameters these processes should be observable. Obviously, from the nature of these multi-Cooper pair processes, one expects these tunneling events to give a sizable contribution to the current when these structures are highly transparent. To illustrate this idea, we show in Fig. 2 the evolution of the sextet Fourier coefficients with the level position ϵ_0 . By moving the level position away from the Fermi energy ($\epsilon_0 = 0$), the magnitude of these coefficients diminishes monotonically towards the tunnel regime, as expected. In this evolution, the ABS spectrum exhibit zero energy states when the level position lies at the Fermi energy, see Fig. 1(d), and they move progressively towards the gap edges when the quantum dot level moves outside the gap (not shown here). The results shown in Fig. 2 also illustrate the fact that in the symmetric case in which all dot-electrode couplings are equal, the sextet coefficients S_2, S_3 , and S_4 are equal, as suggested by the analytical results of Eq. 4. Notice also that the quartet associated to the coefficient S_1 has a magnitude that is 3 times larger than that of the other three sextets, again as expected from the analytical results in this case.

III. SEXTETS AND ABS HYBRIDIZATION: TWO-DOT MODEL

In most experimental situations there are several ABSs that significantly contribute to the supercurrent. Those ABSs, in turn, may hybridize. This occurs when several terminals are coherently coupled. Since this is the situation in which sextets are expected to appear, one may wonder about the connection between ABS hybridization and sextets. To address this issue, we investigate now the simplest model that includes ABS hybridization, namely a two-dot system coupled to four superconducting leads, see Fig. 3(a). The key parameters of this model are described in this figure and again, we neglect interaction effects in the quantum dots. The most important parameter for the following discussion is the hybridization parameter or interdot coupling t , which in this four-terminal configuration controls the degree of hybridization between the two three-terminal ABSs states that may appear in this system (states involving terminals 1, 2, and 4 and 3, 2, and 4). The calculation of the supercurrent can be done in this case following the general recipe described in Appendix A. Again, one can show that the generic CPR of Eq. 3 applies to any four-terminal device and we have again four sextets, which can be identified in exactly the same way from the knowledge of the CPR.

In Fig. 3(b), we show a particular example of the CPR in a high-transparent situation (see figure caption for the list of parameters). We also show in panel (d) the corresponding contribution of the four sextets. Again, this contribution is clearly sizable, providing a clear demonstration of the existence of this type of process. The corresponding ABSs for this example are shown in Fig. 3(c), where only the two states below the Fermi energy are displayed (recall that there is always electron-hole symmetry in our systems).

To address the issue on the connection between sextets and ABS hybridization, we explore the evolution of the magnitude of the sextets with the interdot hopping, t . This evolution is shown in Fig. 4(a) for the same parameters (other than t) as in Fig. 3(b). There are several salient features. First, for $t = 0$, i.e., when there is no hybridization between the ABSs, the sextet contributions exactly vanish, as expected. This illustrates that the hybridization of the bound states requires the occurrence of sextets, or in other words, the sextets are the origin of the ABS hybridization. Notice that the opposite is not true, i.e., the occurrence of sextets does not necessarily imply ABS hybridization, as is obvious in the single-dot model of the previous section. Second, for very large values of t (larger than the couplings of the dots with the electrodes), the sextet amplitudes also tend to vanish. This is a simple consequence of the fact that in this limit a low transparent regime is achieved in which multi-Cooper pair tunneling events become very unlikely. Third, the nonvanishing coefficients reach their maximum around $t \sim \Gamma = 5\Delta$. One can show that this

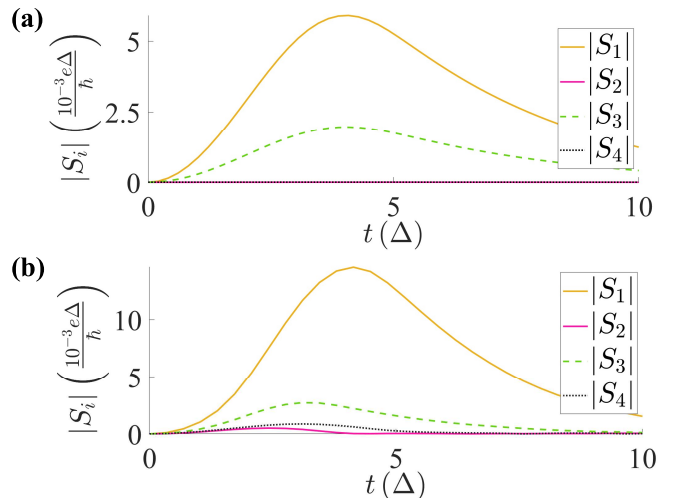


FIG. 4. (a) Evolution of the magnitude of the sextet coefficients as a function of the interdot coupling t in the two-dot model of Fig. 3(a). The parameters other than t are the same as in Fig. 3(b). (b) The same as in (a), but for asymmetric couplings: $\Gamma_1 = 5\Delta$, $\Gamma_{21} = 2\Delta$, $\Gamma_{22} = 3\Delta$, $\Gamma_3 = 4\Delta$, $\Gamma_{41} = 2.5\Delta$ and $\Gamma_{42} = 4\Delta$.

situation corresponds to the highest transparent situation in which zero-energy ABSs become possible, due to a reflectionless scattering mode present in the normal state scattering matrix of the system [55].

Finally, it is also worth noting that the sextets related to terminals 2 and 4 (S_2 and S_4) are exactly zero for the very symmetric configuration of Fig. 4(a). We attribute this cancellation to destructive interference between the different paths that contribute to those two processes. This cancellation can be explicitly shown in a perturbative expansion, where one finds that the contribution is only exactly zero, when the system is fully symmetric and the dot energies are exactly zero. To back this up, we have studied the evolution of the sextets in a situation in which the two couplings to terminals 2 and 4 are not identical, and the results are illustrated in Fig. 4(b). Notice that now all sextets give a finite contribution (for $t \neq 0$), which supports our interpretation above.

IV. SEXTETS IN A REALISTIC SETUP

The previous sections were based on simple models that allowed us to illustrate the nature of sextets and their connection to the ABS hybridization. The last issue that we would like to address is the possibility to have sextets in realistic setups. For this purpose, we investigate now the model described in Fig. 5(a) which we recently employed to describe the results of the tunneling spectroscopy in a four-terminal device fabricated in a hybrid Al/InAs heterostructure [41]. In that work, the first tunneling spectroscopy of ABSs in a four-terminal device was reported in which three different superconduct-

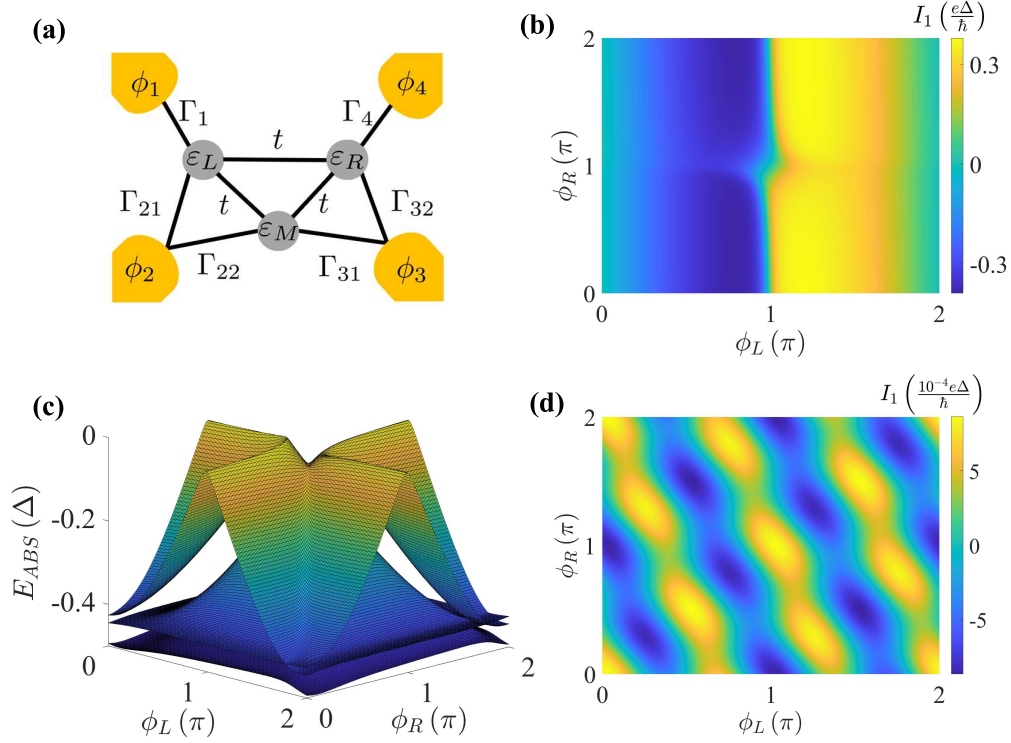


FIG. 5. (a) Schematics of the three-dot model taken from Ref. [41]. Three single-level quantum dots of energies ϵ_L , ϵ_M , and ϵ_R are coupled to four superconducting terminals with phases ϕ_j . We define $\phi_L = \phi_2 - \phi_1$, $\phi_M = \phi_3 - \phi_2$, and $\phi_R = \phi_4 - \phi_3$. The parameters Γ describe the strength of the coupling between the levels and the leads, as shown in this schematics. The parameter t describes the interdot coupling and controls the degree of hybridization of the ABSs. We assume that all interdot couplings are equal. (b) Example of the current-phase relation I_1 for the model in (a) with four identical leads with energy gap Δ . The different parameters are: $\Gamma_j = 0.37\Delta$ for $j \in \{1, 21, 22, 3, 41, 42\}$, $\epsilon_L = \epsilon_M = \epsilon_R = 0.005\Delta$, $t = 0.12\Delta$, $\phi_M = 0.21\pi$, and $k_B T = 0.01\Delta$. (c) The corresponding phase dependence of the ABSs for the example in (b). We only show here the three states below the Fermi energy (there is electron-hole symmetry). (d) The total contribution of the four sextets to the current I_1 in the example of panel (b).

ing phases were independently controlled. Furthermore, signatures of an Andreev tri-molecule were found where ABSs depend on all three superconducting phase differences. On the other hand, the model of Fig. 5(a) containing three dots was shown to explain the key experimental observations concerning the phase dependence of the three low-energy ABSs exhibited by this four-terminal Josephson junction. Moreover, this model was used to argue that under the experimental conditions a phase-controlled topological phase transition could take place. The question arises: does this model predict the occurrence of sextets in this MTJJ?

We show in Fig. 5(b) an example of the CPR for the values used in Ref. [41] to describe the experimental results. We have slightly modified our notation to make it consistent with that of Ref. [41] and we now express the CPR in terms of the following three phase differences: $\phi_L = \phi_2 - \phi_1$, $\phi_M = \phi_3 - \phi_2$, and $\phi_R = \phi_4 - \phi_3$. Notice that this CPR only differs from a CPR of two independent ABSs in the region around (π, π) , in which the states are expected to hybridize the most. The corresponding ABSs computed with this model and for the

same set of parameters are shown in Fig. 5(c). Notice in particular that the highest-energy state only shows signs of hybridization in the region (π, π) mentioned above, which explains the behavior of the CPR. More importantly, Fig. 5(d) displays the corresponding contribution of the sextets to the CPR. These results demonstrate that such processes are present in this multiterminal junction, which further confirms the formation of an Andreev tri-molecule demonstrated in Ref. [41].

It is interesting to mention that the low-energy physics of this model can be studied with the help of an effective Hamiltonian, which can be derived from the full Green's function approach by simply focusing on low energies, see Appendix B for details. This low-energy approximation is convenient, for instance, to analyze the topological nature of the ABSs, as shown in Ref. [41]. Here, we have used this semi-analytical approach to confirm the main conclusions above for the CPR, the contribution of the sextets and the phase-dependence of the ABSs, see details in Appendix B.

For completeness, we have also studied for this model the evolution of the magnitude of the sextets as a func-

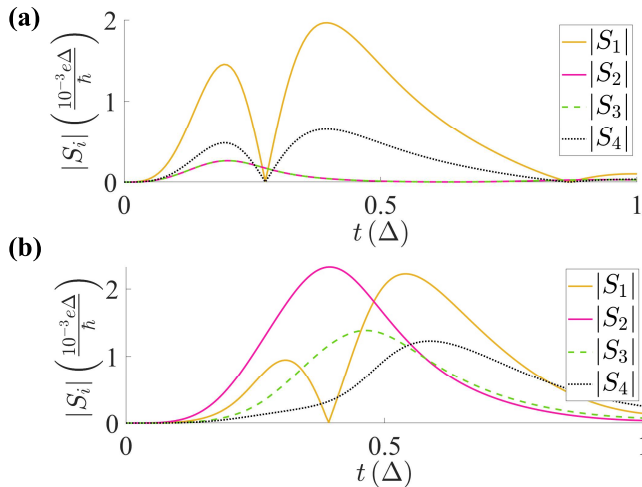


FIG. 6. (a) Evolution of the magnitude of the sextet coefficients as a function of the interdot coupling t in the three-dot model of Fig. 5(a). The parameters other than t are the same as in Fig. 5(b). (b) The same as in (a), but for asymmetric couplings: $\Gamma_1 = 0.37\Delta$, $\Gamma_{21} = 0.5\Delta$, $\Gamma_{22} = 0.25\Delta$, $\Gamma_{31} = 0.75\Delta$, $\Gamma_{32} = 0.45\Delta$ and $\Gamma_4 = 0.8\Delta$.

tion of the hybridization parameter. We show in Fig. 6(a) this evolution for the set of parameters of the example in Fig. 5(b). As expected, the sextet contributions tend to vanish in the two limiting cases: $t \rightarrow 0$ and $t \rightarrow \infty$. Notice that the evolution of these coefficients is not completely monotonic, again suggesting the impact of interference effects. Notably, the contributions $S_{1/4}$ have a sign change in their amplitude and go to zero at a non-zero value of the hybridization. Interestingly, in the vicinity of this hybridization value, there is a topological phase boundary where Weyl nodes originate [55], indicating that there might be a direct connection between sextet contributions and the underlying topology. It should also be noted that two of the coefficients are degenerate (S_2 and S_3). Again, this degeneracy can be lifted by asymmetrizing the couplings to those two leads, as we demonstrate in Fig. 6(b).

V. CONCLUSIONS

In summary, motivated by recent experiments, we have presented in this work a theoretical analysis of the occurrence of sextets in four-terminal Josephson junctions. The analysis of these multi-Cooper pair tunneling processes provides an unambiguous way, at least from the theory side, to determine whether a MTTJ exhibits genuine multiterminal physics. Using simple models in combination with Green's function techniques, we have studied the conditions for the occurrence of these processes and how they can be identified in the analysis of the CPR. We have also shown that they are closely related to the hybridization of ABSs in these heterostructures.

Moreover, we have studied the possible occurrence of sextets in recent experiments realized in hybrid Al/InAs heterostructures [41]. Our analysis supports the idea that such four-terminal devices indeed feature sextets.

Our study here can be extended in many different directions. For instance, following Ref. [54], it is straightforward to analyze the impact of sextets in the ABS spectra of these four-terminal superconducting devices. Another interesting topic is the possible influence of the spin-orbit interaction in these multi-Cooper pair tunneling processes, an interaction that under certain circumstances can indeed affect the ABS spectra of hybrid structures based on semiconductor two-dimensional electron gases [56]. Most interestingly, the connection between non-trivial topology and sextet processes is still not clear. Considering that non-trivial topology only becomes possible in true 4-terminal MTJJs, the existence of sextet processes is a necessary condition for the existence of topology. Furthermore, we find direct signatures that for certain sextet contributions, a sign change with a zero crossing appears which might be related to topological phase boundaries. Exploring this circumstance further could provide a useful tool for experimentalists in investigating the possible connection of the topological properties of the ABS spectra and sextets. Last but not least, it would also be desirable to investigate the role of interactions in the occurrence of sextets and related processes.

ACKNOWLEDGMENTS

We acknowledge fruitful discussions with Valentin Wilhelm. D.C.O. and W.B. acknowledge support by the Deutsche Forschungsgemeinschaft (DFG; German Research Foundation) via SFB 1432 (Project No. 425217212). J.C.C. thanks the DFG and SFB 1432 for sponsoring his stay at the University of Konstanz as a Mercator Fellow.

Appendix A: Green's function formalism: Supercurrent and ABSs

In this appendix, we provide the technical details for the calculation of the supercurrent and the ABS spectrum in the different models discussed in the main text. To give a unified description that can be applied to all these models, we consider a generic MTJJ with N superconducting leads coupled by a central normal region formed by M interconnected single-level quantum dots. Such a system can be described by the following Hamiltonian

$$\hat{H} = \sum_{j=1}^N \hat{H}_{L,j} + \hat{H}_C + \hat{H}_{LC}. \quad (\text{A1})$$

Here, $\hat{H}_{L,j}$ is the BCS Hamiltonian of lead j given by

$$\begin{aligned} \hat{H}_{L,j} = & \sum_{\mathbf{k},\sigma} \epsilon_{\mathbf{k}j} \hat{c}_{\mathbf{k}j\sigma}^\dagger \hat{c}_{\mathbf{k}j\sigma} \\ & + \sum_{\mathbf{k}} \left(|\Delta_j| e^{i\phi_j} \hat{c}_{\mathbf{k}j\uparrow}^\dagger \hat{c}_{-\mathbf{k}j\downarrow}^\dagger + |\Delta_j| e^{-i\phi_j} \hat{c}_{-\mathbf{k}j\downarrow} \hat{c}_{\mathbf{k}j\uparrow} \right), \end{aligned} \quad (\text{A2})$$

where $\hat{c}_{\mathbf{k}j\sigma}^\dagger$ and $\hat{c}_{\mathbf{k}j\sigma}$ are the creation and annihilation operators, respectively, of an electron in state \mathbf{k} , in lead j and with spin σ . Moreover, $|\Delta_j|$ is the magnitude of the order parameter of lead j and ϕ_j is the corresponding phase. On the other hand, \hat{H}_C is the Hamiltonian of the central region that adopts the form

$$\hat{H}_C = \sum_{i,\sigma} \varepsilon_i \hat{d}_{i\sigma}^\dagger \hat{d}_{i\sigma} + \sum_{ij,\sigma} t_{ij} \hat{d}_{i\sigma}^\dagger \hat{d}_{j\sigma}, \quad (\text{A3})$$

where $\hat{d}_{i\sigma}^\dagger$ and $\hat{d}_{i\sigma}$ are the creation and annihilation operators, respectively, of an electron in quantum dot i and spin σ . By defining $\tilde{d}^\dagger = (\hat{d}_{1\uparrow}^\dagger, \hat{d}_{1\downarrow}^\dagger, \dots, \hat{d}_{M\uparrow}^\dagger, \hat{d}_{M\downarrow}^\dagger)$, we can rewrite the Hamiltonian of the central region as $\hat{H}_C = \tilde{d}^\dagger \bar{H}_C \tilde{d}$, where \bar{H}_C is given by

$$\bar{H}_C = \begin{pmatrix} \epsilon_1 & 0 & t_{12} & 0 & \cdots & t_{1M} & 0 \\ 0 & -\epsilon_1 & 0 & -t_{12} & \cdots & 0 & -t_{1M} \\ t_{21} & 0 & \epsilon_2 & 0 & \cdots & t_{2M} & 0 \\ 0 & -t_{21} & 0 & -\epsilon_2 & \cdots & 0 & -t_{2M} \\ \vdots & \vdots & \vdots & \vdots & \ddots & \vdots & \vdots \\ t_{M1} & 0 & \cdots & t_{MM-1} & 0 & \epsilon_M & 0 \\ 0 & -t_{M1} & \cdots & 0 & -t_{MM-1} & 0 & -\epsilon_M \end{pmatrix}. \quad (\text{A4})$$

Finally, \hat{H}_{LC} describes the coupling between the central region and the superconducting leads and reads

$$\hat{H}_{LC} = \sum_{ij,\mathbf{k},\sigma} w_{ij} \left(\hat{d}_{i\sigma}^\dagger \hat{c}_{\mathbf{k}j\sigma} + \hat{c}_{\mathbf{k}j\sigma}^\dagger \hat{d}_{i\sigma} \right), \quad (\text{A5})$$

where w_{ij} is the tunneling matrix element between lead i and dot j , which we assume to be real and independent of \mathbf{k} . Related to these matrix elements, we define the tunneling rates $\Gamma_{ij} = \pi N_{0i} w_{ij}^2$, where N_{0i} is the normal density of states at the Fermi energy of lead i .

Our goal now is to compute the supercurrent flowing, for instance, through terminal 1. The corresponding current density operator is given by

$$\hat{I}_1(t) = \frac{ie}{\hbar} \sum_{\mathbf{k},j,\sigma} w_{1j} \left(\hat{c}_{\mathbf{k}1\sigma}^\dagger(t) \hat{d}_{j\sigma}(t) - \hat{d}_{j\sigma}^\dagger(t) \hat{c}_{\mathbf{k}1\sigma}(t) \right). \quad (\text{A6})$$

Next, we use the definition of the lesser Green's functions within the Nambu representation:

$$\hat{G}_{ij}^{+-}(t, t') = -i \sum_{\mathbf{k}} \left\langle \hat{T}_C \left\{ \hat{c}_{\mathbf{k}i}(t_+) \tilde{d}_j^\dagger(t_-) \right\} \right\rangle, \quad (\text{A7})$$

where \hat{T}_C is the time-ordering operator on the Keldysh contour and we have defined the spinors $\tilde{c}_{\mathbf{k}i}^\dagger =$

$(c_{\mathbf{k}i\uparrow}^\dagger, c_{-\mathbf{k}i\downarrow})$ and $\tilde{d}_j^\dagger = (d_{j\uparrow}^\dagger, d_{j\downarrow}^\dagger)$. In terms of these Green's functions, the expectation value $I_1 = \langle \hat{I}_1 \rangle$ can be written as

$$I_1 = \frac{e}{\hbar} \sum_j \text{Tr} \left\{ \hat{\tau}_3 \left(\hat{V}_{j1} \hat{G}_{1j}^{+-}(t, t) - \hat{G}_{j1}^{+-}(t, t) \hat{V}_{1j} \right) \right\}, \quad (\text{A8})$$

where Tr denotes the trace in Nambu space, $\hat{\tau}_3$ is the third Pauli matrix in that space, and we have defined

$$\hat{V}_{1j} = \hat{V}_{j1} = \begin{pmatrix} w_{1j} & 0 \\ 0 & -w_{1j} \end{pmatrix}. \quad (\text{A9})$$

Since we are interested in the supercurrent, the system is in equilibrium and the Green's functions only depend on the difference of the time arguments. Thus, we can Fourier transform the Green's functions to energy space and rewrite the current as

$$I_1 = \frac{e}{\hbar} \sum_j \int_{-\infty}^{\infty} dE \text{Tr} \left\{ \hat{\tau}_3 \left[\hat{V}_{j1} \hat{G}_{1j}^{+-}(E) - \hat{G}_{j1}^{+-}(E) \hat{V}_{1j} \right] \right\}. \quad (\text{A10})$$

Moreover, we can make use of the equilibrium relation

$$\hat{G}^{+-}(E) = [\hat{G}^a(E) - \hat{G}^r(E)] n_F(E), \quad (\text{A11})$$

where $n_F(E)$ is the Fermi function, to rewrite the lesser Green's functions in terms of the retarded and advanced ones.

To compute the different Green's functions we follow a perturbative approach in which we assume that the whole system is divided into different subsystems, namely the leads and the central normal region formed by the array of dots. We consider the couplings between leads and the central system as the perturbation. With this choice, the Green's functions can be calculated by solving the corresponding Dyson's equations. Thus, for instance, we can compute the retarded and advanced Green's functions that enter into the current expression using the following Dyson's equations

$$\hat{G}_{j1}^{r,a} = \sum_i \hat{G}_{ji}^{r,a} \hat{V}_{i1} \hat{g}_1^{r,a} \quad \text{and} \quad \hat{G}_{1j}^{r,a} = \sum_i \hat{g}_1^{r,a} \hat{V}_{1i} \hat{G}_{ij}^{r,a}, \quad (\text{A12})$$

where \hat{g} denotes the unperturbed Green's functions. Using these relations, together with Eq. (A11), we can rewrite the current as

$$I_1 = \frac{e}{\hbar} \int_{-\infty}^{\infty} \text{Tr}' \left\{ \bar{\tau}_3 \left([\bar{\Sigma}_1^a, \bar{G}_C^a] - [\bar{\Sigma}_1^r, \bar{G}_C^r] \right) \right\} n_F(E) dE, \quad (\text{A13})$$

where $(\bar{})$ indicates that the corresponding quantity is a $2M \times 2M$ matrix in the combined Nambu and dot space and Tr' represents the trace in this combined space. Moreover, $\bar{\tau}_3 = \hat{\tau}_3 \otimes \hat{1}_M$, where $\hat{1}_M$ is the $M \times M$ unit matrix, and the different 2×2 blocks of the self-energy $\bar{\Sigma}_l^{r,a}$, corresponding to lead l , are defined as

$$[\bar{\Sigma}_l^{r,a}]_{ij}(E) = \hat{V}_{il} \hat{g}_l^{r,a}(E) \hat{V}_{lj}. \quad (\text{A14})$$

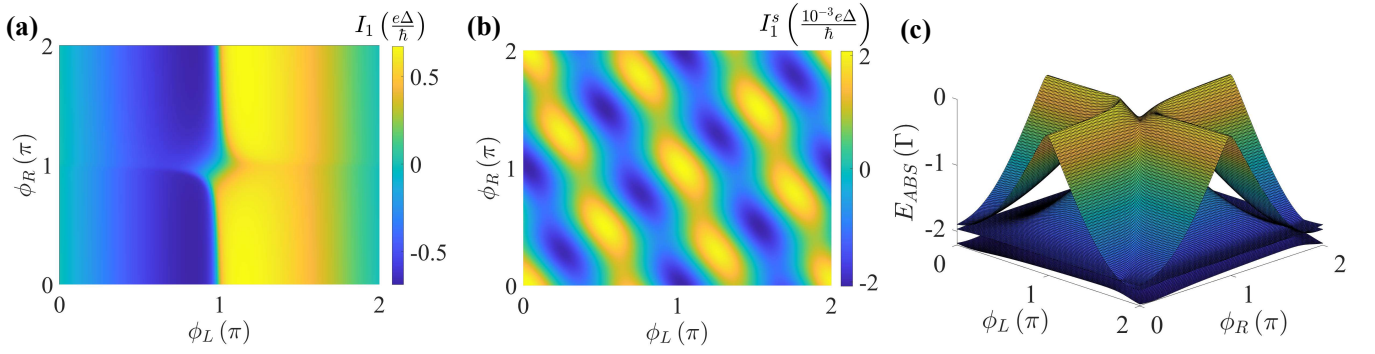


FIG. 7. (a) Current-phase relation I_1 for the model in Fig. 5(a) using the effective Hamiltonian approximation. The different parameters are those used in Fig. 5(b). (b) The total contribution of the four sextets to the current I_1 in the example of panel (b) using the effective Hamiltonian approximation. (c) The phase dependence of the ABSs for the example in (a) obtained diagonalizing the corresponding effective Hamiltonian. We only show here the three states below the Fermi energy (there is electron-hole symmetry).

Here, $\hat{g}_l^{r,a}$ are the Green's function of lead l given by

$$\begin{aligned} \hat{g}_l^{r,a}(E) &\equiv \begin{pmatrix} g_l^{r,a} & f_l^{r/a} e^{i\varphi_l} \\ f_l^{r/a} e^{-i\varphi_l} & g_l^{r,a} \end{pmatrix} \\ &= \frac{-1}{\sqrt{|\Delta_l|^2 - (E \pm \eta)^2}} \begin{pmatrix} E \pm \eta & |\Delta_l| e^{i\varphi_l} \\ |\Delta_l| e^{-i\varphi_l} & E \pm \eta \end{pmatrix}, \end{aligned} \quad (\text{A15})$$

where E is the energy and $\eta = 0^+$.

Using $\hat{G}^r = (\hat{G}^a)^\dagger$, we can express Eq. (A13) as

$$I_1 = \frac{2e}{h} \int_{-\infty}^{\infty} \Re(\text{Tr}' \{ \bar{\tau}_3 [\bar{\Sigma}_1^a, \bar{G}_C^a] \}) n_F(E) dE. \quad (\text{A16})$$

The last step now is to compute \hat{G}_C^a , which can be obtained from the following Dyson's equation

$$\hat{G}_C^a = \left[(E - i\eta)\bar{1} - \bar{H}_C - \sum_l \bar{\Sigma}_l \right]^{-1}. \quad (\text{A17})$$

This is the general recipe that can be applied to any of the models in the main text. In the case of the single-dot model of Sec. II, it is straightforward to show that this recipe leads to Eqs. (1) and (2) for the supercurrent through lead 1.

Let us now briefly discuss how to identify the sextet contributions in the CPR, focusing on the single-dot model of Sec. II with four terminals. The denominator that appears in the current expression of Eq. (1), which is defined in Eq. (2), can be written as $D = (E^2 - \epsilon_0^2)[1 - x]$, where

$$\begin{aligned} x = \frac{1}{(E^2 - \epsilon_0^2)} &\left\{ \sum_j \Gamma_j^2 + 2E \sum_j \Gamma_j g_j^a + \right. \\ &\left. 2 \sum_{\langle jk \rangle} \Gamma_j \Gamma_k [f_j^a f_k^a \cos(\phi_{jk}) - g_j^a g_k^a] \right\}, \end{aligned} \quad (\text{A18})$$

Here, $\sum_{\langle jk \rangle}$ indicates a sum over all possible pair of leads with $j \neq k$. Thus, $1/D$ can be written as

$$\frac{1}{D} = \frac{1}{(E^2 - \epsilon_0^2)} \frac{1}{1 - x} = \frac{1}{(E^2 - \epsilon_0^2)} \sum_{n=0}^{\infty} x^n. \quad (\text{A19})$$

The terms in the current proportional to x^2 include the sextet contributions to the leading order (sixth order in the Γ 's). In particular, after straightforward manipulations, one can identify the following contributions

$$\begin{aligned} I_1^s &= 3A_1 \sin(\phi_2 + \phi_3 + \phi_4 - 3\phi_1) \\ &\quad - A_2 \sin(\phi_1 + \phi_3 + \phi_4 - 3\phi_2) \\ &\quad - A_3 \sin(\phi_1 + \phi_2 + \phi_4 - 3\phi_3) \\ &\quad - A_4 \sin(\phi_1 + \phi_2 + \phi_3 - 3\phi_4), \end{aligned} \quad (\text{A20})$$

where the coefficients A_i are defined in Eq. (4).

Appendix B: Effective Hamiltonian approximation

As mentioned in the main text, it is often convenient to derive an effective Hamiltonian to describe the low-energy physics of all the models considered in this work. In particular, that is very useful for the analysis of the topological properties of the ABSs, see e.g. Ref. [41]. This effective Hamiltonian can be derived from Eq. (A17) by simply taking the limit $E \rightarrow 0$ as follows

$$\bar{H}_{\text{eff}} = \bar{H}_C + \sum_j \bar{\Sigma}_j(E=0). \quad (\text{B1})$$

From this Hamiltonian, the ABS spectrum can be obtained by diagonalizing it, while the CPR can be computed from the knowledge of the phase-dependence of the ABS energies by using Eq. (5).

Obviously, this approximation cannot be expected to reproduce the physics of the ABSs for high energies close to the gap. In any case, it provides useful insight and

allows us to test the basic properties of both the CPR and the ABS spectra. As an example, we show in Fig. 7 the results for both the CPR and the ABSs for the three-dot model of Sec. IV and for the same parameters as in Fig. 5. Notice that in this case the energy of the ABSs

is normalized by the coupling Γ since the gap Δ is considered to be infinite in this approximation. In any case, one can see that this approximation nicely reproduces all the salient features discussed in Sec. IV.

-
- [1] B. Josephson, Phys. Lett. **1**, 251 (1962).
 - [2] A. Barone and G. Paterno, *Physics and Applications of the Josephson Effect* (John Wiley & Sons, Inc., 1982).
 - [3] C. W. J. Beenakker and H. van Houten, Phys. Rev. Lett. **66**, 3056 (1991).
 - [4] A. Furusaki and M. Tsukada, Phys. Rev. B **43**, 10164 (1991).
 - [5] J.-D. Pillet, C. H. L. Quay, P. Morfin, C. Bena, A. L. Yeyati, and P. Joyez, Nat. Phys. **6**, 965 (2010).
 - [6] W. Chang, V. E. Manucharyan, T. S. Jespersen, J. Nygård, and C. M. Marcus, Phys. Rev. Lett. **110**, 217005 (2013).
 - [7] L. Bretheau, Ç. Ö. Girit, H. Pothier, D. Esteve, and C. Urbina, Nature **499**, 312 (2013).
 - [8] L. Bretheau, Ç. Ö. Girit, C. Urbina, D. Esteve, and H. Pothier, Phys. Rev. X **3**, 041034 (2013).
 - [9] C. Janvier, L. Tosi, L. Bretheau, Ç. Ö. Girit, M. Stern, P. Bertet, P. Joyez, D. Vion, D. Esteve, M. F. Goffman, H. Pothier, and C. Urbina, Science **349**, 1199 (2015).
 - [10] L. Bretheau, J. I.-J. Wang, R. Pisoni, K. Watanabe, T. Taniguchi, and P. Jarillo-Herrero, Nat. Phys. **13**, 756 (2017).
 - [11] D. J. van Woerkom, A. Proutski, B. van Heck, D. Bouman, J. I. Väyrynen, L. I. Glazman, P. Krogstrup, J. Nygård, L. P. Kouwenhoven, and A. Geresdi, Nat. Phys. **13**, 876 (2017).
 - [12] M. Hays, G. de Lange, K. Serniak, D. J. van Woerkom, D. Bouman, P. Krogstrup, J. Nygård, A. Geresdi, and M. H. Devoret, Phys. Rev. Lett. **121**, 047001 (2018).
 - [13] L. Tosi, C. Metzger, M. F. Goffman, C. Urbina, H. Pothier, S. Park, A. L. Yeyati, J. Nygård, and P. Krogstrup, Phys. Rev. X **9**, 011010 (2019).
 - [14] F. Nichele, E. Portolés, A. Fornieri, A. M. Whiticar, A. C. C. Drachmann, S. Gronin, T. Wang, G. C. Gardner, C. Thomas, A. T. Hatke, M. J. Manfra, and C. M. Marcus, Phys. Rev. Lett. **124**, 226801 (2020).
 - [15] M. Hays, V. Fatemi, K. Serniak, D. Bouman, S. Diamond, G. de Lange, P. Krogstrup, J. Nygård, A. Geresdi, and M. H. Devoret, Nat. Phys. **16**, 1103 (2020).
 - [16] M. Hays, V. Fatemi, D. Bouman, J. Cerrillo, S. Diamond, K. Serniak, T. Connolly, P. Krogstrup, J. Nygård, A. Levy Yeyati, A. Geresdi, and M. H. Devoret, Science **373**, 430 (2021).
 - [17] M. Pita-Vidal, A. Bargerbos, R. Žitko, L. J. Splitthoff, L. Grünhaupt, J. J. Wesdorp, Y. Liu, L. P. Kouwenhoven, R. Aguado, B. van Heck, A. Kou, and C. K. Andersen, Nat. Phys. **19**, 1110 (2023).
 - [18] M. Hinderling, D. Sabonis, S. Paredes, D. Z. Haxell, M. Coraiola, S. C. ten Kate, E. Cheah, F. Krizek, R. Schott, W. Wegscheider, and F. Nichele, Phys. Rev. Appl. **19**, 054026 (2023).
 - [19] J. J. Wesdorp, F. J. Matute-Cañadas, A. Vaartjes, L. Grünhaupt, T. Laeven, S. Roelofs, L. J. Splitthoff, M. Pita-Vidal, A. Bargerbos, D. J. van Woerkom, P. Krogstrup, L. P. Kouwenhoven, C. K. Andersen, A. L. Yeyati, B. van Heck, and G. de Lange, Phys. Rev. B (2023).
 - [20] A. W. Draelos, M.-T. Wei, A. Seredinski, H. Li, Y. Mehta, K. Watanabe, T. Taniguchi, I. V. Borzenets, F. Amet, and G. Finkelstein, Nano Lett. **19**, 1039 (2019).
 - [21] G. V. Graziano, J. S. Lee, M. Pendharkar, C. J. Palmstrøm, and V. S. Pribiag, Phys. Rev. B **101**, 054510 (2020).
 - [22] N. Pankratova, H. Lee, R. Kuzmin, K. Wickramasinghe, W. Mayer, J. Yuan, M. G. Vavilov, J. Shabani, and V. E. Manucharyan, Phys. Rev. X **10**, 031051 (2020).
 - [23] E. G. Arnault, T. F. Q. Larson, A. Seredinski, L. Zhao, S. Idris, A. McConnell, K. Watanabe, T. Taniguchi, I. Borzenets, F. Amet, and G. Finkelstein, Nano Lett. **21**, 9668 (2021).
 - [24] G. V. Graziano, M. Gupta, M. Pendharkar, J. T. Dong, C. P. Dempsey, C. Palmstrøm, and V. S. Pribiag, Nat. Commun. **13**, 5933 (2022).
 - [25] M. Gupta, G. V. Graziano, M. Pendharkar, J. T. Dong, C. P. Dempsey, C. Palmstrøm, and V. S. Pribiag, Nat. Commun. **14**, 3078 (2023).
 - [26] T. Yokoyama and Y. V. Nazarov, Phys. Rev. B **92**, 155437 (2015).
 - [27] R.-P. Riwar, M. Houzet, J. S. Meyer, and Y. V. Nazarov, Nat. Commun. **7**, 11167 (2016).
 - [28] E. Eriksson, R.-P. Riwar, M. Houzet, J. S. Meyer, and Y. V. Nazarov, Phys. Rev. B **95**, 075417 (2017).
 - [29] J. S. Meyer and M. Houzet, Phys. Rev. Lett. **119**, 136807 (2017).
 - [30] H.-Y. Xie, M. G. Vavilov, and A. Levchenko, Phys. Rev. B **96**, 161406(R) (2017).
 - [31] H.-Y. Xie and A. Levchenko, Phys. Rev. B **99**, 094519 (2019).
 - [32] E. V. Repin, Y. Chen, and Y. V. Nazarov, Phys. Rev. B **99**, 165414 (2019).
 - [33] L. Peralta Gavensky, G. Usaj, and C. A. Balseiro, Phys. Rev. B **100**, 014514 (2019).
 - [34] M. Houzet and J. S. Meyer, Phys. Rev. B **100**, 014521 (2019).
 - [35] R. L. Klees, G. Rastelli, J. C. Cuevas, and W. Belzig, Phys. Rev. Lett. **124**, 197002 (2020).
 - [36] H. Weisbrich, R. L. Klees, G. Rastelli, and W. Belzig, PRX Quantum **2**, 010310 (2021).
 - [37] H.-Y. Xie, J. Hasan, and A. Levchenko, Phys. Rev. B **105**, L241404 (2022).
 - [38] H. Barakov and Y. V. Nazarov, Phys. Rev. B **107**, 014507 (2023).
 - [39] L. Teshler, H. Weisbrich, J. Sturm, R. L. Klees, G. Rastelli, and W. Belzig, SciPost Phys. **15**, 214 (2023).
 - [40] M. Coraiola, D. Z. Haxell, D. Sabonis, H. Weisbrich, A. E. Svetogorov, M. Hinderling, S. C. ten Kate, E. Cheah, F. Krizek, R. Schott, W. Wegscheider, J. C. Cuevas, W. Belzig, and F. Nichele, Nat. Commun. **14**,

- 6784 (2023).
- [41] T. Antonelli, M. Coraiola, D. C. Ohnmacht, A. E. Svetogorov, D. Sabonis, S. C. ten Kate, E. Cheah, F. Krizek, R. Schott, J. C. Cuevas, W. Belzig, W. Wegscheider, and F. Nichele, Exploring the energy spectrum of a four-terminal josephson junction: Towards topological andreev band structures (2025), arXiv:2501.07982 [cond-mat.mes-hall].
 - [42] M. Coraiola, A. E. Svetogorov, D. Z. Haxell, D. Sabonis, M. Hinderling, S. C. Ten Kate, E. Cheah, F. Krizek, R. Schott, W. Wegscheider, *et al.*, ACS Nano **18**, 9221 (2024).
 - [43] D. C. Ohnmacht, V. Wilhelm, H. Weisbrich, and W. Belzig, Phys. Rev. Lett. **134**, 156601 (2025).
 - [44] A. Freyn, B. Douçot, D. Feinberg, and R. Mélin, Phys. Rev. Lett. **106**, 257005 (2011).
 - [45] T. Jonckheere, J. Rech, T. Martin, B. Douçot, D. Feinberg, and R. Mélin, Phys. Rev. B **87**, 214501 (2013).
 - [46] J. Rech, T. Jonckheere, T. Martin, B. Douçot, D. Feinberg, and R. Mélin, Phys. Rev. B **90**, 075419 (2014).
 - [47] D. Feinberg, T. Jonckheere, J. Rech, T. Martin, B. Douçot, and R. Mélin, Eur. Phys. J. B **88**, 99 (2015).
 - [48] A. Melo, V. Fatemi, and A. R. Akhmerov, SciPost Phys. **12**, 017 (2022).
 - [49] R. Mélin, R. Danneau, and C. B. Winkelmann, Phys. Rev. Res. **5**, 033124 (2023).
 - [50] A. H. Pfeffer, J. E. Duvauchelle, H. Courtois, R. Mélin, D. Feinberg, and F. Lefloch, Phys. Rev. B **90**, 075401 (2014).
 - [51] Y. Cohen, Y. Ronen, J.-H. Kang, M. Heiblum, D. Feinberg, R. Mélin, and H. Shtrikman, Proc. Natl. Acad. Sci. U.S.A. **115**, 6991 (2018).
 - [52] K.-F. Huang, Y. Ronen, R. Mélin, D. Feinberg, K. Watanabe, T. Taniguchi, and P. Kim, Nat. Commun. **13**, 3032 (2022).
 - [53] E. G. Arnault, S. Idris, A. McConnell, L. Zhao, T. F. Larson, K. Watanabe, T. Taniguchi, G. Finkelstein, and F. Amet, Nano Lett. **22**, 7073 (2022).
 - [54] D. C. Ohnmacht, M. Coraiola, J. J. García-Esteban, D. Sabonis, F. Nichele, W. Belzig, and J. C. Cuevas, Phys. Rev. B **109**, L241407 (2024).
 - [55] D. C. Ohnmacht, V. Wilhelm, and W. Belzig, Reflectionless modes as a source of Weyl nodes in multiterminal Josephson junctions (2025), arXiv:2503.10874 [cond-mat].
 - [56] M. Coraiola, D. Z. Haxell, D. Sabonis, M. Hinderling, S. C. t. Kate, E. Cheah, F. Krizek, R. Schott, W. Wegscheider, and F. Nichele, Phys. Rev. X **14**, 031024 (2024).